Graph Matching Based on Stochastic Perturbation

Chengcai Leng[1,2,3], Wei Xu[2], Irene Cheng[3], *Senior Member, IEEE*, Anup Basu[3], *Senior Member, IEEE*

[1]*Key Laboratory of Nondestructive Testing, Ministry of Education, School of Mathematics and Information Sciences, Nanchang Hangkong University, Nanchang 330063, China;*
[2]*Department of Applied Mathematics, Northwestern Polytechnical University, Xi'an 710072, China;*
[3]*Department of Computing Science, University of Alberta, Edmonton, AB T6G 2H1, Canada*
chengcaileng@gmail.com, weixu@nwpu.edu.cn, locheng@ualberta.ca, basu@ualberta.ca

Abstract: This paper presents a novel perspective on characterizing the spectral correspondence between nodes of weighted graphs for image matching applications. The algorithm is based on the principal feature components obtained by stochastic perturbation of a graph. There are three areas of contributions in this work. First, a stochastic normalized Laplacian matrix of a weighted graph is obtained by perturbing the matrix of a sensed graph model. Second, we obtain the eigenvectors based on an eigen-decomposition approach, where representative elements of each row of this matrix can be considered to be feature components of a feature point. Third, correct correspondences are determined in a low-dimensional principal feature component space between the graphs. In order to further enhance image matching, we also exploit the random sample consensus (RANSAC) algorithm, as a post-processing step, to eliminate mismatches in feature correspondences. Experiments on synthetic and real-world images demonstrate the effectiveness and accuracy of the proposed method.

Keywords: graph matching; image matching; stochastic perturbation; principal feature component; random sample consensus (RANSAC)

1. Introduction

Graphs are commonly used as abstract descriptions in the literature for numerous computer vision and pattern recognition problems that can be formulated as graph

matching problems [1]. Examples include graph matching [2-5], image segmentation [6-7], shape recognition [8-12], and shape segmentation and registration [13]. The problem of graph matching can be reduced to finding a mapping between nodes of two graphs that preserves most of the similarity relationship between the nodes. Image matching can be transformed into a graph matching problem because of the representational power of graphs, which use nodes to represent local features extracted from the image, and edges to depict relational aspects between features [14-15]. Graph matching algorithms in the literature can be broadly divided into spectral methods [16-23], relaxation and probabilistic methods [24-29], projection clustering methods [30-32], RANSAC-based methods [33-34], diffeomorphic demons methods [35-36] and other methods [37-38], according to the optimization criteria used. Relaxation and probabilistic methods define probability distributions for the relational errors and optimize using discrete relaxation algorithms. Projection clustering methods project the vertices of a graph into an eigenspace to find the correspondence in that eigenspace. Large rigid motion matching, iteratively based on local features, using RANSAC as a post-processing step, is also employed. However, these approaches lack global consideration.

Spectral graph theory is a powerful tool aimed at characterizing the global structural properties of graphs using the eigenvalues and eigenvectors of either the adjacency matrix or the closely related normalized Laplacian matrix [39]. This theory is effective in analyzing geometric distribution of feature points and in solving computer vision problems, such as graph matching [40-41]. Among spectral approaches, Umeyama [2] proposed a formulation for same size graphs, which derives the minimum difference permutation matrix by singular value decomposition techniques. Following the ideas from structural chemistry, Scott and Longuet-Higgins [3] introduced a Gaussian weighted function to build an inter-image proximity matrix between feature points in different images being matched. Then, they performed singular value decomposition on the resulting matrix in order to get correspondences from the strength matrix; an approach that can accommodate point sets of different sizes. However, their method is sensitive to view rotation. To overcome this

disadvantage, Shapiro and Brady [4] constructed an intra-image proximity matrix for the individual point sets being matched to capture relational image structures. However, a sign correction stage is necessary in [4]. Since then, a number of enhancements and new ideas have been put forward by researchers. Gold and Rangarajan [5] exploited a soft assign update algorithm for graph matching. Carcassoni and Hancock [16] embedded the modal structure of point sets into the expectation maximization (EM) framework, and improved the accuracy of correspondences. Cross and Hancock [25] presented graph matching in the EM framework by introducing a dual-step EM algorithm; however, their method cannot guarantee the global optimal. Luo and Hancock [26] combined the EM algorithm with singular value decomposition to improve the matching. Zass and Shashua [27] proposed the hyper-graph matching problem in a probabilistic setting represented by a convex optimization. Cho and Lee [29] proposed a progressive method to update candidate matches by exploiting a move of graphs via probabilistic voting, which greatly boosts the objective function in an integer quadratic programming problem. However, its computational complexity is high because exploring the full matching space is required [42]. Caelli and Kosibov [31] sought correspondences by searching for a match that maximizes the inner product of the truncated and renormalized eigenvectors. Learning graph matching is proposed by Caetano et al. [43] to estimate a compatibility function, such that the solution of the resulting graph matching problem best matches the expected solution. Recently, Ma et al. have published a series of papers [44-48] on feature matching based on the assumption that the point matches undergo a coherent transformation which can be iteratively estimated by the expectation maximization (EM) algorithm [49]. They presented a unified framework for non-rigid feature matching based on a reproducing kernel Hilbert space. The underlying transformation between the point pairs is represented using a displacement field in [44-45], and using a Gaussian mixture model in [46-48].

Although the above methods have their own merits, the main limitation is their inability to cope with far from isomorphic cases. Also, these approaches may not work well in nearly isomorphic cases; implying that they cannot be used when significant

levels of structural corruption and noise are present. In addition, sign correction is often needed in order to make both sets of axes have consistent directions. These methods usually suffer from the combinatorial problem where computing an exact or similar match has exponential cost in terms of the number of nodes in the graph. Motivated by these problems, we propose a novel graph matching method by stochastic perturbation, incorporating RANSAC as a post-processing step, to achieve the best possible match in a low dimensional principal feature component graph for image registration. We apply the ideas behind matrix perturbation analysis [50], i.e., the bigger eigenvalues corresponding to eigenvectors are relatively stable to small perturbations, while the smaller eigenvalues are sensitive to small perturbations. First, we add a small perturbation on eigenvalues of a normalized Laplacian matrix of the sensed graph to get the optimized graph (isomorphic cases). Then, we obtain the eigenvectors based on eigen-decomposition, which can be regarded as a modal matrix. The modal matrix is orthogonal, and has the eigenvectors as its column vectors. Each row of a modal matrix can be considered as a feature vector of a feature, i.e., representative elements of each row are the principal feature components of a feature, and columns can be considered as modal coordinates of features. Finally, we can efficiently find the correct correspondences in a low dimensional principal feature component space between the graphs. We can further eliminate part of the feature correspondences by incorporating RANSAC [33] as a post-processing step. The proposed method can resolve the drawbacks of previous approaches (i.e., not performing well in nearly isomorphic cases, sensitivity to the amount of rotation, and requiring sign correction) and can reduce the dimensional complexity inherited from combinatorial computations. Experimental results show that the proposed method outperforms Umeyama's [2] method, Shapiro and Brady's method [4], and the method of Zass [27]. In this paper, we also extend our previous work [20] on image registration to formulate the theoretic model.

The rest of this paper is organized as follows. Section 2 gives a theoretical analysis of the graph matching problem. A novel matching algorithm based on the principal feature component of a weighted graph with stochastic perturbation is

proposed in Section 3. Section 4 describes the experimental results, and we conclude and outline some directions for future research in Section 5.

2. Formulation of the graph matching theoretical model

Given an $m \times l$ image I, let $N = m \times l$, and $V = \{v_1, v_2, v_3, \cdots, v_N\}$ denote the full set of pixels in the image I, where v_i denotes the i^{th} pixel of I. Based on the set V, we construct a weighted undirected graph $G(V, E, W)$ with V as the node set and $E = V \times V$ as the edge set. For simplicity, an edge $e \in E$ spanning two nodes v_i and v_j, is denoted by e_{ij}. $W = (w_{ij})$ is a weighted function which gives a real non-negative value $w(v_i, v_j)$ to each pair of nodes v_i and v_j, whose elements are weights of edges denoted by w_{ij}, where the weight w_{ij} on edge e_{ij} is a measure of the similarity between nodes v_i and v_j.

Definition 1 (Adjacency Matrix): The adjacency matrix of a weighted graph $G = (V, E, W)$ is a $N \times N$ matrix A_G defined as follows:

$$A_G = \left[a_{ij} \right] = \begin{cases} w(v_i, v_j) & i \neq j \\ 0 & else \end{cases} \tag{1}$$

where G is a weighted undirected graph, A_G is a symmetric matrix, the degree of a vertex $v_i \in V$ is defined as $d_i = \sum_{j=1}^{n} w_{ij}$ and the degree matrix D is defined as the diagonal matrix with degrees $d_1, \cdots, d_N$, i.e., $D = diag(d_1, d_2, \cdots, d_N)$. Let us define the Laplacian matrix L of the graph as follows:

$$L = \left[l_{ij} \right] = D - A_G = \begin{cases} -\left\| v_i - v_j \right\|^2 & i \neq j \\ d_i & i = j \end{cases} \quad i, j = 1, 2, \cdots, N \tag{2}$$

where $w_{ij} = w(v_i, v_j) = \left\| v_i - v_j \right\|^2$, $i, j = 1, 2, \cdots, N$, and $d_i = d_{v_i} = \sum_{j=1}^{N} \left\| v_i - v_j \right\|^2$, $i = 1, 2, \cdots, N$.

The normalized Laplacian matrix is defined as follow:

$$\hat{L} = D^{-\frac{1}{2}} L D^{-\frac{1}{2}} = D^{-\frac{1}{2}} (D - A_G) D^{-\frac{1}{2}} \tag{3}$$

The normalized Laplacian matrix $\hat{L}$ (to simplify the notation $\hat{L}$ is written as L from this point onward) is positive semi-definite and thus has positive or zero eigenvalues, which are desirable properties of the graph Laplacian matrix [40]. By exploiting this concept, we establish that the normalized graph Laplacian matrix is positive semi-definite and has N non-negative real-valued eigenvalues $0 = \lambda_1 \le \lambda_2 \le \cdots \lambda_N$.

2.1 Stochastic perturbation analysis

Graph matching is the process of finding a correspondence between the nodes and edges of graphs that satisfies (more or less stringent) constraints ensuring that similar substructures in one graph are mapped to similar substructures in the other. However, graph matching can be transformed into a problem of Laplacian matrix matching. The correspondence between the eigenvectors of a Laplacian matrix is defined following Umeyama's approach [2] using a permutation matrix P. In fact, exact isomorphism [51] occurs rarely. Very often the graphs being compared are obtained as the result of a description process that is inevitably subject to some form of noise. Thus, missing or extra nodes and edges can appear, hampering the isomorphism. In this paper, we adjust the structure of a sensed graph by perturbation in order to maximize correspondences between the feature points for image matching. In order to improve matching performance, we propose using matrix perturbation analysis to obtain an approximate optimized weighted graph by an optimal parameter. Let L_G and L_H be the normalized Laplacian matrices of two graphs to be matched. We consider the normalized Laplacian matrix L_G, and the perturbation matrix L_{HH}, where L_{HH} can be obtained from L_H with some stochastic perturbation. The perturbation normalized Laplacian matrix L_{HH} is given by:

$$L_{HH} = L_H + \omega * Random, \tag{4}$$

where *Random* (random number uniformly distributed in the range of (0,1)) is a stochastic matrix, and ω is a parameter, which can adjust the structure of the sensed weighted graph by solving an optimization problem. That is, the perturbation L_{HH} is very similar to L_G (approximate isomorphic case).

The problem of matching two normalized Laplacian matrices L_G and L_H of graphs G and H is transformed into the problem of matching L_G and L_{HH}. We use the following measure of difference:

$$J(R) = \min_R \left\| RL_G R^T - L_{HH} \right\|_F^2, \tag{5}$$

The approximate optimized normalized Laplacian matrix L_{HH} can be obtained by an optimal parameter ω based on matrix perturbation analysis (Theorem 1), i.e., the problem of isomorphism of L_G and L_H is transformed into an approximate isomorphic case of L_G and L_{HH}.

The following theorem extends the theorem in [20].

Theorem 1: Let L_G and L_H be $N \times N$ (real) symmetric normalized Laplacian matrices with N non-negative eigenvalues $\alpha_1 \geq \alpha_2 \geq \cdots \geq \alpha_N$ and $\beta_1 \geq \beta_2 \geq \cdots \geq \beta_N$, respectively, and $L_{HH} = L_H + \omega * Random$ obtained by perturbing L_H, their singular value decomposition being given by:

$$L_G = U_G \Lambda_G U_G^T, \tag{6}$$

$$L_H = V_H \Lambda_H V_H^T, \tag{7}$$

$$Random = V_H' \Lambda_H' V_H'^T, \tag{8}$$

where U_G, V_H, and V_H' are orthogonal matrices, $\Lambda_G = diag(\alpha_1, \alpha_2, \cdots, \alpha_N)$, $\Lambda_H = diag(\beta_1, \beta_2, \cdots, \beta_N)$, $\Lambda_H' = diag(\gamma_1, \gamma_2, \cdots, \gamma_N)$. $L_{HH} = V_{HH} \Lambda_{HH} V_{HH}^T$, where V_{HH} is an orthogonal matrix, and $\Lambda_{HH} = diag(\beta_1 + \omega\gamma_1, \beta_2 + \omega\gamma_2, \cdots, \beta_N + \omega\gamma_N)$.

Then:

$$J(P)=\min_{P}\left\|PL_{G}P^{T}-L_{H}\right\|_{F}^{2}\Leftrightarrow J(R)=\min_{R}\left\|RL_{G}R^{T}-L_{HH}\right\|_{F}^{2}$$
$$\Leftrightarrow J(\omega)=\min_{\omega}\sum_{i=1}^{N}\left(\alpha_{i}-\left(\beta_{i}+\omega\gamma_{i}\right)\right)^{2}, \tag{9}$$

where $R=V_{HH}SU_{G}^{T}=\hat{V}_{HH}U_{G}^{T}$ is a permutation matrix, and S is a sign matrix.

Proof: Starting with the optimization problem in Eq. (9), we have:

$$\begin{aligned}
&J(P)=\min_{P}\left\|PL_{G}P^{T}-L_{HH}\right\|_{F}^{2}\\
&\Leftrightarrow J(R)=\min_{R}\left\|RL_{G}R^{T}-L_{HH}\right\|_{F}^{2}\\
&=\left\|RU_{G}\Lambda_{G}U_{G}^{T}R^{T}-V_{HH}\Lambda_{HH}V_{HH}^{T}\right\|_{F}^{2}\\
&=\left\|V_{HH}^{T}RU_{G}\Lambda_{G}U_{G}^{T}R^{T}V_{HH}-\Lambda_{HH}\right\|_{F}^{2}\\
&=\left\|V_{HH}^{T}V_{HH}SU_{G}^{T}U_{G}\Lambda_{G}U_{G}^{T}U_{G}S^{T}V_{HH}^{T}V_{HH}-\Lambda_{HH}\right\|_{F}^{2}\\
&=\left\|S\Lambda_{G}S^{T}-\Lambda_{HH}\right\|_{F}^{2}\\
&=\left\|\Lambda_{G}-\Lambda_{HH}\right\|_{F}^{2}\\
&=\sum_{i=1}^{N}\left(\alpha_{i}-\left(\beta_{i}+\omega\gamma_{i}\right)\right)^{2}
\end{aligned}$$

Thus,

$$J(R)=\min_{R}\left\|RL_{G}R^{T}-L_{HH}\right\|^{2}\Leftrightarrow J(\omega)=\min_{\omega}\sum_{i=1}^{N}\left(\alpha_{i}-\left(\beta_{i}+\omega\gamma_{i}\right)\right)^{2}. \tag{10}$$

The optimal parameter ω is obtained by minimizing $J(\omega)$ to zero, and then the approximate optimized weighted graph (normalized Laplacian matrix) L_{HH} is obtained by Eq. (4). ■

2.2 Analysis of principal feature component on a weighted graph

We perform singular value decomposition of L_{G} and L_{HH}, i.e., $L_{G}=U_{G}\Lambda_{G}U_{G}^{T}$, $L_{HH}=V_{HH}\Lambda_{HH}V_{HH}^{T}$. The modal matrices U_{G} and V_{HH} are orthogonal, and each row of U_{G} and V_{HH} can be considered to be feature vectors $F_{U_{G}}$ and $F_{V_{HH}}$, respectively. We extract some elements (the first few, more specifically 3, biggest eigenvalues corresponding to column eigenvectors are used as explained below) from each row of

U_G and V_{HH}, which are regarded as principal feature components of a weighted graph. This way, we construct a matching matrix $\left(Z_{ij}\right)_{N\times N}$ based on modal matrices U_G and V_{HH}, i.e.,

$$\left(Z_{ij}\right)_{N\times N}=\left(\left\|F_{ir}-F_{jr}\right\|^2\right)_{N\times N} \tag{11}$$

where r is the principal feature component of a weighted graph, F_{ir} and F_{jr} are i^{th} principal feature component of U_G and j^{th} principal feature component of V_{HH}, respectively.

A "few" non-repeated eigenvalues in descending order are selected corresponding to the column eigenvectors used. In the current implementation, we tested a range of principal feature component values r of a weighted graph, and found that the best results can be achieved when $r=3$. Thus, 3 biggest values are selected. Automatically choosing the principal feature components of feature points is another challenging problem in image matching that we will address in future work. The advantages of exploiting principal feature components include: First, to characterize the structure of the original data and discard the less important components reducing the size of the data structure. Second, a sign correction stage is not needed, which eliminates the maximum consistency of the features of U_G and V_{HH} as much as possible.

3. Matching algorithm based on principal feature component of weighted graph with stochastic perturbation

Based on the model formulation given in the previous section, we detail the steps of our matching algorithm as follows:

1. Given two point sets, construct the normalized Laplacian matrices L_G and L_H of point sets G and H respectively, following Eq. (3).

2. Compute perturbation matrix L_{HH} by stochastic perturbation of L_H following Eq. (4).
3. Perform singular value decomposition of L_G, L_H, and *Random* (defined in Section 2.1) respectively, to get the orthogonal matrices U_G, V_H, and V_H' of point sets G and H.
4. Use Eq. (10) to seek an optimal parameter ω, namely minimize Eq. (10) to zero, to obtain the optimized perturbation matrix L_{HH}.
5. Perform singular value decomposition of L_G and L_{HH}, i.e., $L_G = U_G \Lambda_G U_G^T$, and $L_{HH} = V_{HH} \Lambda_{HH} V_{HH}^T$.
6. Compute the distance between a reference principal feature component of graph G and a sensed principal feature component of graph H by $\left(Z_{ij}\right)_{N\times N} = \left(\left\|F_{ir} - F_{jr}\right\|^2\right)_{N\times N}$ based on Eq. (11), where Z_{ij} reflects the similarity between these two sets of features. Best matches are given based on the elements of Z_{ij} being both the smallest in its row and the smallest in its column; we then regard the two different features G_i and H_j as having a 1:1 correspondence with one another.
7. The RANSAC post-processing step can be incorporated in order to further enhance feature correspondence in image matching.
8. Both affine and projective transform can be used. Since affine transform is more commonly used in applications, we apply affine transform for illustration and compute the transform parameters by matching relationships, and align the reference image and sensed image based on the transform parameters.

4. Experimental results and performance evaluations

In this section, we first show the results of our novel image matching technique based on principal feature components of weighted stochastic perturbation, and then

provide both qualitative and quantitative evaluations to verify the effectiveness of our technique compared to other methods. We commence with synthetic images and real-world environments, to demonstrate the robustness under view changes, including temporal changes, and the presence of outliers. In the second part, we evaluate the proposed method with image sequences and real-world images, to demonstrate that our method outperforms other alternatives, including the condition of illumination variations, remote sensing images and different medical image modalities. In the current implementation, we tested a range of principal feature component values r of a weighted graph, and found that the best results can be achieved when $r = 3$. Thus, three non-repeated eigenvalues in descending order are selected corresponding to the column eigenvectors used. We will investigate how to obtain an optimal r value in future work. All the experiments have been done on a personal computer using MATLAB R2010a, with Intel(R) Core (TM) CPU 2.53GHz and 4.00GB RAM.

4.1 Robustness under view changes and outliers

Synthetic images

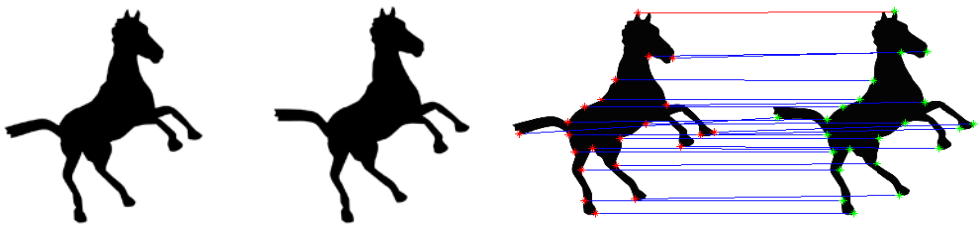

(a) Reference image (b) Sensed image (c) Matching result

Fig. 1: Matching results of the horse images: (a) reference image, (b) sensed image, and (c) matching result from our method.

Fig. 1 shows experiments using synthetic horse images to test the ability of our algorithm under translations, with (a) the reference image, and (b) the sensed image from a different viewpoint (translated). Twenty-two target feature points are defined in the horse model, including one ear tip, for correspondence matching. Feature points are extracted by the Harris Corner Detector [52] in both the reference and sensed images, based on points of maximum curvature along the contour of the horse.

The matching results show that our method is accurate except for one feature

point, which matches on the wrong ear as shown in Fig. 1 (c) (red color line). Further investigation shows that the mismatch is due to the similar curvature of the horse ears, causing the Harris Corner Detector to detect a different ear as the feature in the sensed image.

Outliers

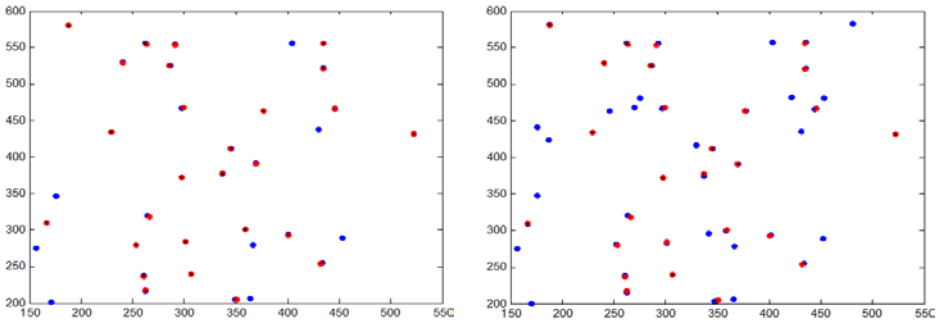

(a) (b)

Fig. 2: Validating our method by adding outliers: (a) is the registration result with 8 outliers discriminated in blue, and (b) has 18 outliers discriminated in blue. The original 27 features points are marked in both red and blue. Our method is able to register the feature points back to their original coordinates accurately.

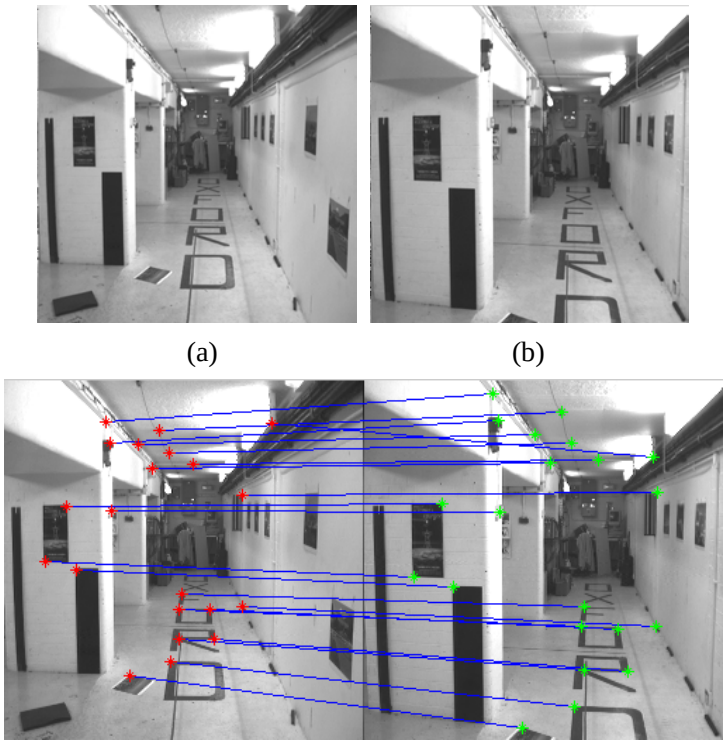

(a) (b)

(c)

Fig. 3: Matching result for the Oxford corridor sequence. (a) Reference image (Frame 1), (b) sensed image (Frame 5), (c) matching result.

To test performance on outliers, we used a synthetic point set containing 27

feature points (reference image). In the first experiment, 8 outliers were added to the feature points, giving a total of 35, which were then transformed using an affine transform to generate the sensed image. Our method was applied to find the correct transformation parameters and we were able to map the feature points back to their original coordinates discriminating the eight outliers. Fig. 2 (a) is the registration result. The zoom-in view clearly shows the 27 features points in both red and blue, and the 8 outliers in blue.

In the second experiment, 18 outliers were added, giving a total of 45 points in the transformed sensed image. Our method was able to find the correct transform parameters and map the feature points back to their original coordinates as shown in Fig. 2 (b). This shows that our method is robust in the presence of outliers.

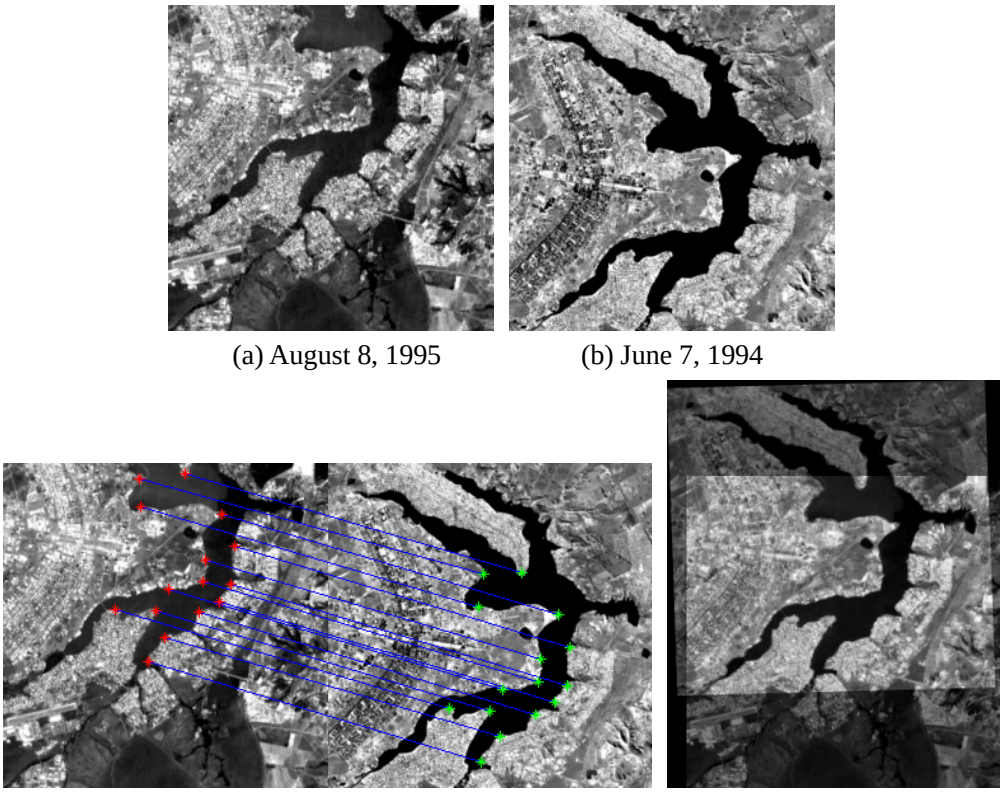

(a) August 8, 1995 (b) June 7, 1994

(c) (d)

Fig. 4: Matching and registration results for urban region remote sensing images. (a) Reference SPOT band 3 image acquired on Aug. 8, 1995. (b) Sensed TM band 4 image acquired on Jun. 7, 1994. (c) Our matching and (d) registration result.

Registration results on a pair of images from multi-view capture, and remote sensing images

We test the application of our method in a multi-view computer vision problem

using two images (Frame 1 and Frame 5) from the Oxford corridor sequence [53] as shown in Fig. 3. Twenty-one landmark feature points are manually identified on these two images as in [43] exploiting the points marked manually to test graph matching performance instead of using the Harris detector.

For applications in remote sensing image registration, fifteen feature points are manually identified on the two aerial images (512×512 images of Brasilia, Brazil), which were taken at different times using different sensors. Fig. 4 (a) and (b) are urban region SPOT band 3 and TM band 4 obtained on August 8, 1995 and June 7, 1994, respectively. Fig. 4 (c) shows the matching result and (d) shows the registration result generated by our method.

We change the structure of the sensed weighted graph by stochastic perturbation, in order to avoid one-to-many correspondences or mismatching. As a result, we are able to accurately find one-to-one correspondences between nodes of two weighted graphs.

4.2 Comparisons and performance evaluations

Image Sequences

Fig. 5 shows comparisons of matching under rotation (about 20 degree) and illumination variations on two frames (the 15^{th} and 45^{th} frame) of the CMU/VASC 111 frame long toy house sequence, and on two frames (the 730_c^{th} and the 730_i110^{th} frame) of object 730 (Amsterdam Library of Object Images), respectively. Matching results using the proposed method are compared with Umeyama's [2] method, Shapiro and Brady's method [4], and the method of Zass [27].

In these experiments, thirty feature points (the 15^{th} and 45^{th} frames in the left column of Fig. 5) and forty points (the 730_c^{th} and the 730_i110^{th} frames in the right column of Fig. 5) are selected using the Harris Corner Detector in the reference and sensed images.

Our method is accurate under rotation and illumination variations and is able to find feature correspondences more accurately than the methods of Umeyama, Shapiro and Brady, and Zass. Table 1 summarizes the performance of our method compared to

these other methods.

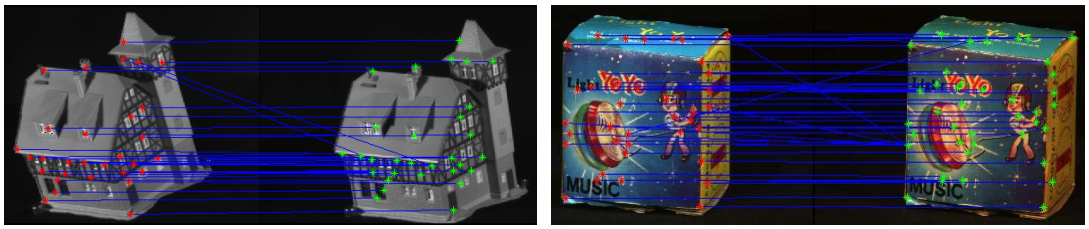

Umeyama's method (a) (b)

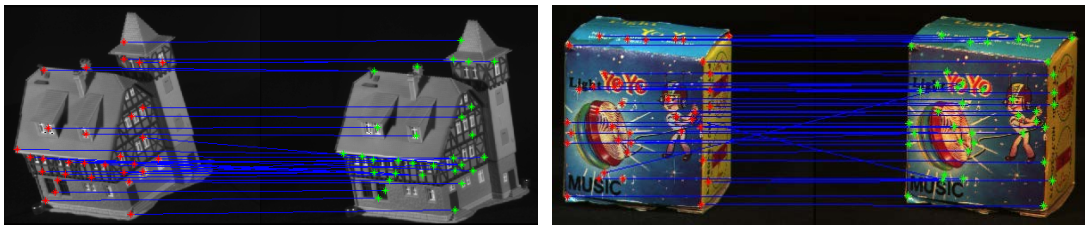

Shapiro and Brady's method (c) (d)

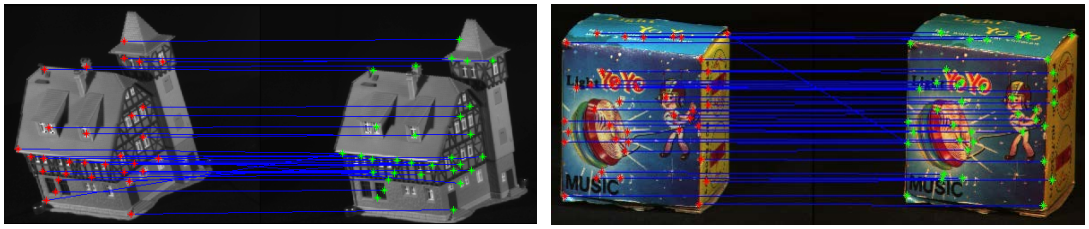

Zass' method (e) (f)

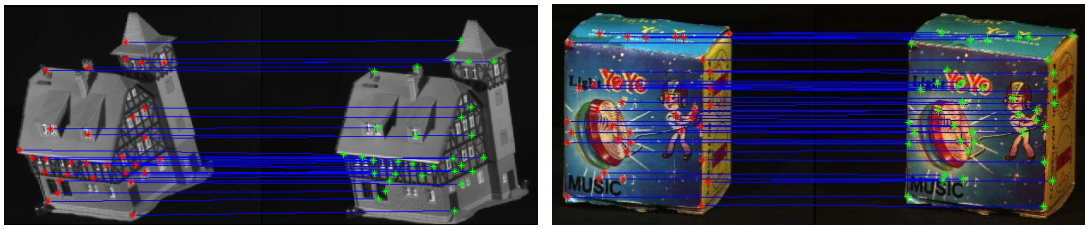

Our method (g) (h)

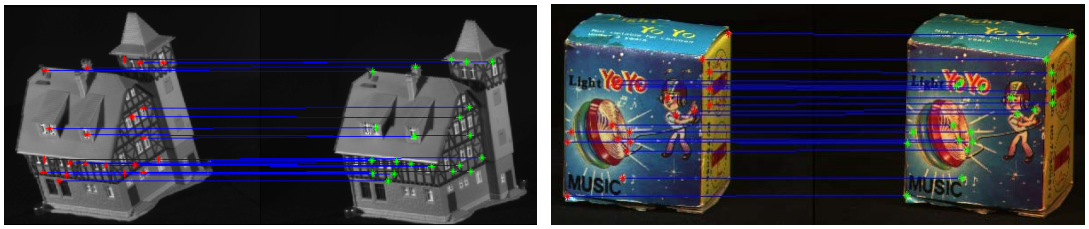

Our method after incorporating the RANSAC step

(i) (j)

Fig. 5: Matching results under rotation and illumination variations. Top row: Umeyama's method; second row: Shapiro and Brady's method; third row: Zass' method; fourth row: our method; bottom row: our method after incorporating the RANSAC step.

Our method performs even better when combined with the RANSAC post-processing step, which eliminates mismatches further. For example, Fig. 5 (i) and (j) eliminate nine and twenty features correspondences in Fig. 5 (g) and (h), respectively, after incorporating the RANSAC step.

Fig. 6 compares the performance of using the algorithms of Umeyama, Shapiro and Brady, Zass, and our method. Feature correspondences in Fig. 6 (a) and (b) reflect the correspondences in the left and right columns of Fig. 5, respectively. We can see that our method outperforms the other methods, which is achieved by exploiting the principal feature component to perturb the weighted graph, making our method more robust and have higher accuracy than the other three methods.

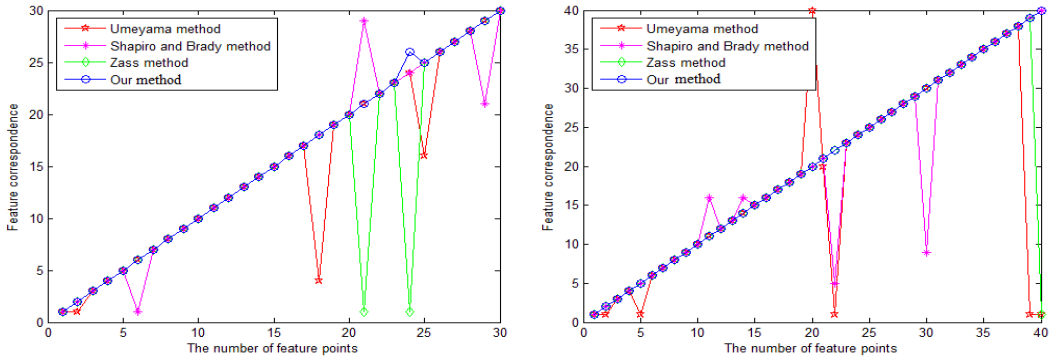

(a) (b)

Fig. 6: Performance comparison of feature correspondences under rotation and illumination variations. Feature correspondence using Umeyama's method, Shapiro and Brady's method, the method of Zass, and our method for (a) the left columns and (b) the right columns of Fig. 5 respectively.

TABLE 1: Summary of Experimental Results for the House Image Sequences and Amsterdam Library of Object Images

# of feature and % matched	15^{th}-45^{th} frame	730_c^{th}-730_i110^{th} frame
Umeyama	27 (90.00%)	35 (87.50%)
Shapiro	27 (90.00%)	36 (90.00%)
Zass	28 (93.33%)	39 (97.50%)
Our method	29 (96.67%)	40 (100.0%)
Our method with RANSAC step	21 (100.0%)	20 (100.0%)

In order to verify the robustness of the proposed method by increasing the number of outliers under big rotation changes (about 45 degrees) on the 5^{th} and 76^{th}

frames of the CMU/VASC 111 frame house sequence, comparisons of matching results under the different outliers compared to Zass' method are shown in Fig. 7. Here the x-axis denotes the number of outliers and the y-axis is the accuracy of matching. We use Zass' method because it outperforms the other two methods on real-image experiments. From the experimental results, the matching performance of both Zass' method and the proposed method decreases with larger number of outliers. However, the proposed method is relatively stable, and can find more candidate points which are correct and good for matching. Also, the accuracy of the proposed method is higher and declines more slowly, and the accuracy is still higher than Zass' method, which indicates that the proposed method is robust to outliers. This is because the principal feature components obtained by perturbation can discriminate outliers, which can be regarded as point features used to improve the robustness.

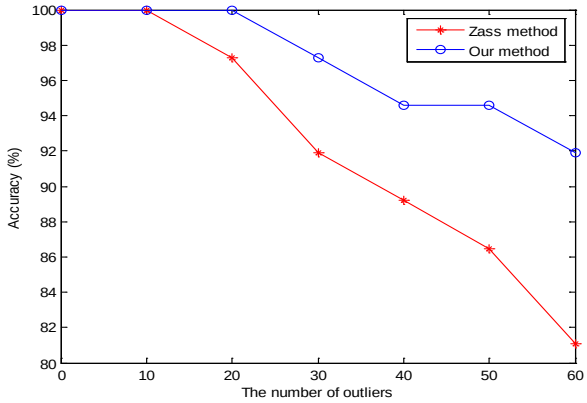

Fig. 7: Comparisons of matching results under different number of outliers.

In order to verify the robustness of the proposed method under different perturbation levels, we added Gaussain noise with mean 0 and different standard deviations σ using the Matlab function (σ.*randn) to the CMU/VASC 111 frame long toy house sequence. We give nine experiments using image pairs from (the 0^{th} and 10^{th} frame), (the 0^{th} and 20^{th} frame) to (the 0^{th} and 90^{th} frame) with feature points automatically detected. Each experiment was repeated 12 times with different standard deviations σ, and fifteen feature points were detected from the 0^{th} frame. Table 2 shows the performance under different Gaussain noise levels. Our method is relatively stable under different perturbation levels, and can find correct

correspondences. These experiments also reveal an interesting relationship, i.e., higher standard deviations correspond to lower perturbation values maintaining good correspondence accuracy. This illustrates why the performance of our method is high. However, when the feature points cannot be detected well because of bigger view changes to house images, matching performance decreases, e.g., between 0^{th} and 50^{th} frame. Fig. 8 shows the matching performance under different noise levels for the different house image frames. In Fig. 8, the y-axis is the accuracy of matching and the x-axis denotes the house frames. We can see that the proposed method is robust to high noise levels.

TABLE 2: Matching Performance under Different Noise Levels for the Different House Image Frames

house	Different standard deviations σ, perturbation parameters (e-004) and correspondences (%)											
	1	2	3	4	5	6	7	8	9	10	11	12
(0^{th},10^{th})	3.1497 100	1.5219 100	1.0728 100	0.8386 100	0.6928 100	0.5315 100	0.4343 100	0.3894 100	0.3625 100	0.3298 100	0.2969 100	0.2704 100
(0^{th},20^{th})	9.8091 100	5.1160 100	3.5747 100	2.2099 100	1.8773 100	1.6565 100	1.4510 100	1.1739 100	1.2211 100	1.0663 100	0.9598 100	0.8554 100
(0^{th},30^{th})	21.000 100	9.2909 100	7.0821 100	4.4676 100	4.1752 100	3.4922 100	2.8707 100	2.0369 100	1.7827 100	1.8822 100	1.7080 100	1.6391 100
(0^{th},40^{th})	4.1809 100	2.1224 100	1.5904 100	1.1351 100	0.7929 100	0.7258 100	0.6670 100	0.5322 100	0.4844 100	0.3943 100	0.3632 100	0.3162 100
(0^{th},50^{th})	1.2381 100	0.6894 100	0.4588 100	0.3410 100	0.2538 100	0.2158 100	0.1903 100	0.1796 100	0.1580 100	0.1466 100	0.1141 100	0.1048 100
(0^{th},60^{th})	10.000 93.33	5.3614 93.33	3.5979 93.33	3.1014 93.33	2.2604 93.33	1.8559 93.33	1.6111 93.33	1.2928 93.33	1.2196 93.33	1.0801 93.33	0.9036 93.33	0.7980 93.33
(0^{th},70^{th})	8.8562 86.67	4.8005 86.67	3.1477 86.67	2.3814 86.67	1.9077 86.67	1.3989 86.67	1.3903 86.67	1.0891 86.67	0.9771 86.67	0.8454 86.67	0.7397 86.67	0.6377 86.67
(0^{th},80^{th})	13.000 86.67	7.1354 86.67	4.5669 86.67	3.5240 86.67	2.8220 86.67	2.3694 86.67	1.9617 86.67	1.5833 86.67	1.4436 86.67	1.2808 86.67	1.2176 86.67	1.1851 86.67
(0^{th},90^{th})	10.000 46.67	5.1308 46.67	3.3860 46.67	2.3839 46.67	2.2974 46.67	1.9216 46.67	1.4604 46.67	1.3914 46.67	1.0608 46.67	0.9697 46.67	0.9523 46.67	0.8948 46.67

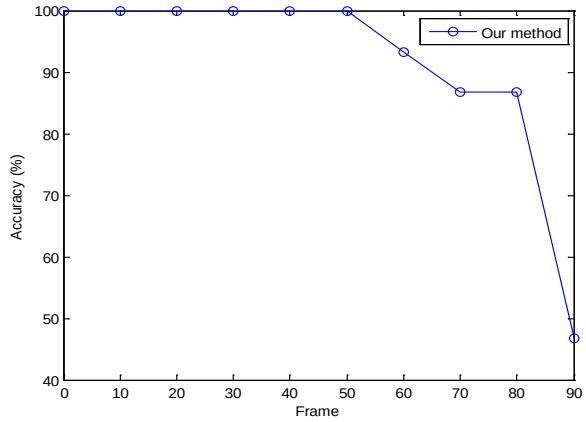

Fig. 8: Plot of accuracy for various noise levels for the different house image frames.

Remote sensing images

Fig. 9 is another example of remote sensing images. We compare our matching results with the other three methods. Two 405×350 images with high temporal changes were used in our experiments. They were both taken from the same area of a trailer park at different times. Forty feature points are extracted by the Harris Corner Detector [52]. Observe that our method outperforms the three alternatives as shown in Fig. 9, and the result of Shapiro and Brady's method is better than that of Umeyama, which demonstrates that a purely structural approach (Umeyama's method) is not robust and unstable for finding correspondences. Shapiro and Brady's method needs to use a sign correction step, which can adversely affect the matching results if the correction is not done accurately. Also, note that Zass' method is better than Umeyama, and Shapiro and Brady by using an iterative successive projection and probabilistic approach. The reason for the success of our method is that we change the structure of the sensed weighted graph by stochastic perturbation in order to improve the structural stability. We exploit the principal feature component space and find the correct one-to-one correspondences between nodes of two weighted graphs in the principal feature component space, which avoids the sign correction step. Furthermore, we can eliminate outliers by incorporating the RANSAC step.

Comparing the matching results in Fig. 9 (a), (c), (e) and (g), it can be observed that the proposed method can find the correct one-to-one correspondences between

nodes of two weighted graphs. The other three methods have features mismatches, which produce incorrect transformation parameters (dark segments in the registration results shown in Fig. 9 (b), (d) and (f)). Before using the RANSAC step, the proposed method is better than the others for feature point matching as shown in Fig. 9 (g) and (h). The RANSAC step is used to achieve more robust image registration by eliminating more mismatches.

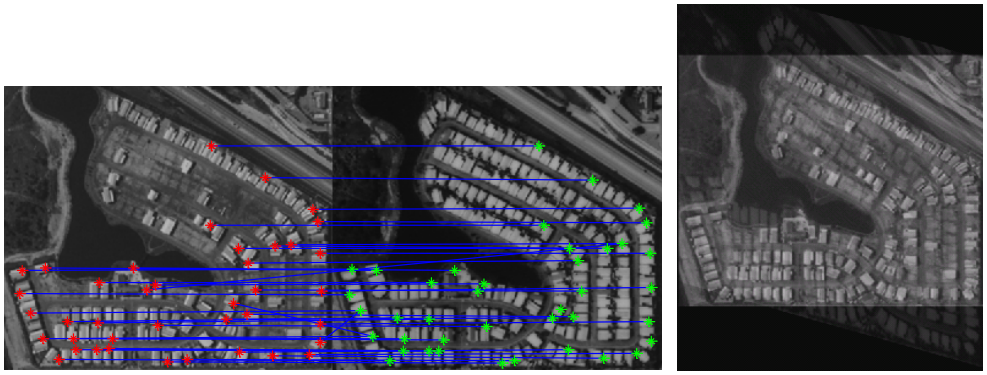

Umeyama's method: darker segments are caused by inaccurate transformation

(a) Matching result (b) Registration

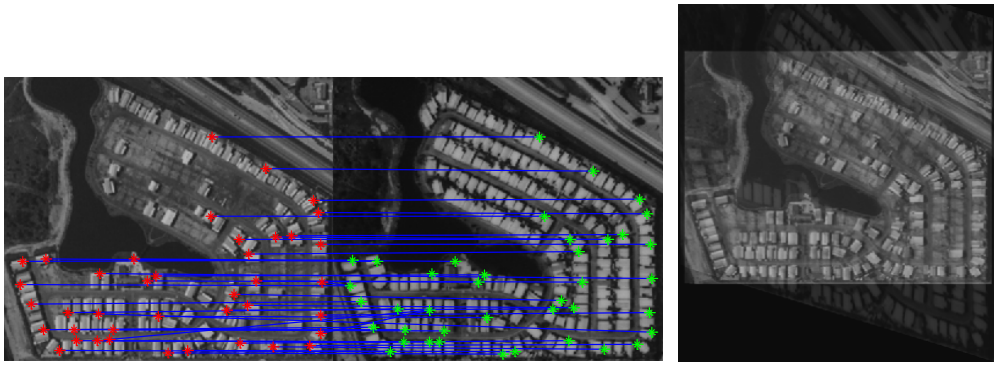

Shapiro and Brady's method: darker segments are caused by inaccurate transformation

(c) Matching result (d) Registration

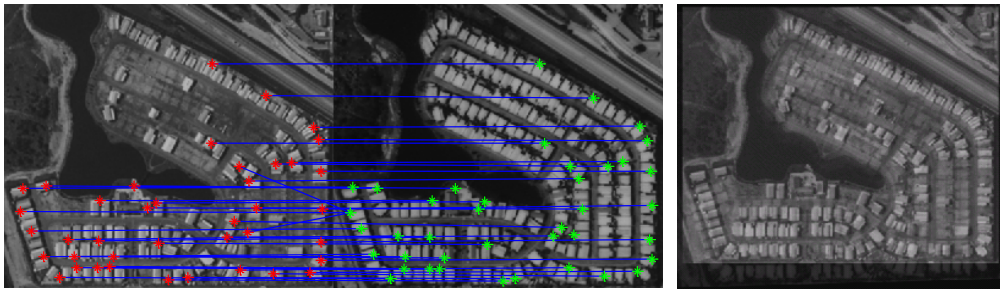

Zass' method: darker segments are caused by inaccurate transformation

(e) Matching result (f) Registration

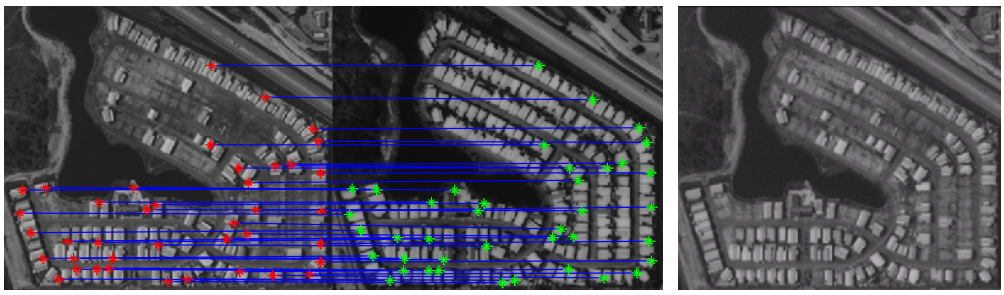

Our method: correct registration is by accurate transformation

(g) Our matching result (h) Registration

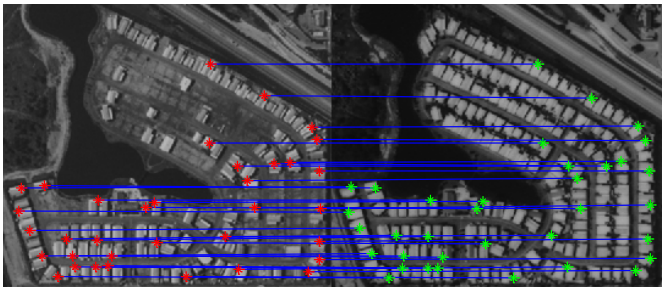

(i) Our matching after incorporating the RANSAC step

Fig. 9: Comparison of matching and registration results using images with high structural changes: (a) and (b) are matching and registration result using Umeyama's method; (c) and (d) are matching and registration result using Shapiro and Brady's method; (e) and (f) are matching and registration result using Zass' method; (g) and (h) are matching and registration result using our method; (i) matching result after incorporating the RANSAC step.

Test on other types of images

(a) ACC method (b) VFC method

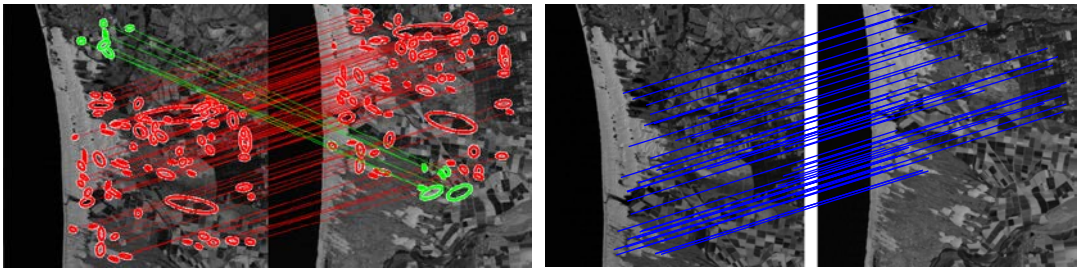

(c) ACC method (d) VFC method

Fig. 10: Comparison of matching results using two types of images: (a) and (c) matching results using ACC method; (b) and (d) matching results using VFC method.

We further compared the proposed method with recent point matching methods including agglomerative correspondence clustering (ACC) method [32], vector field consensus (VFC) method [45] and other feature-based matching methods, such as the SIFT method [54] and the SURF method [55], to test the effectiveness of the proposed method.

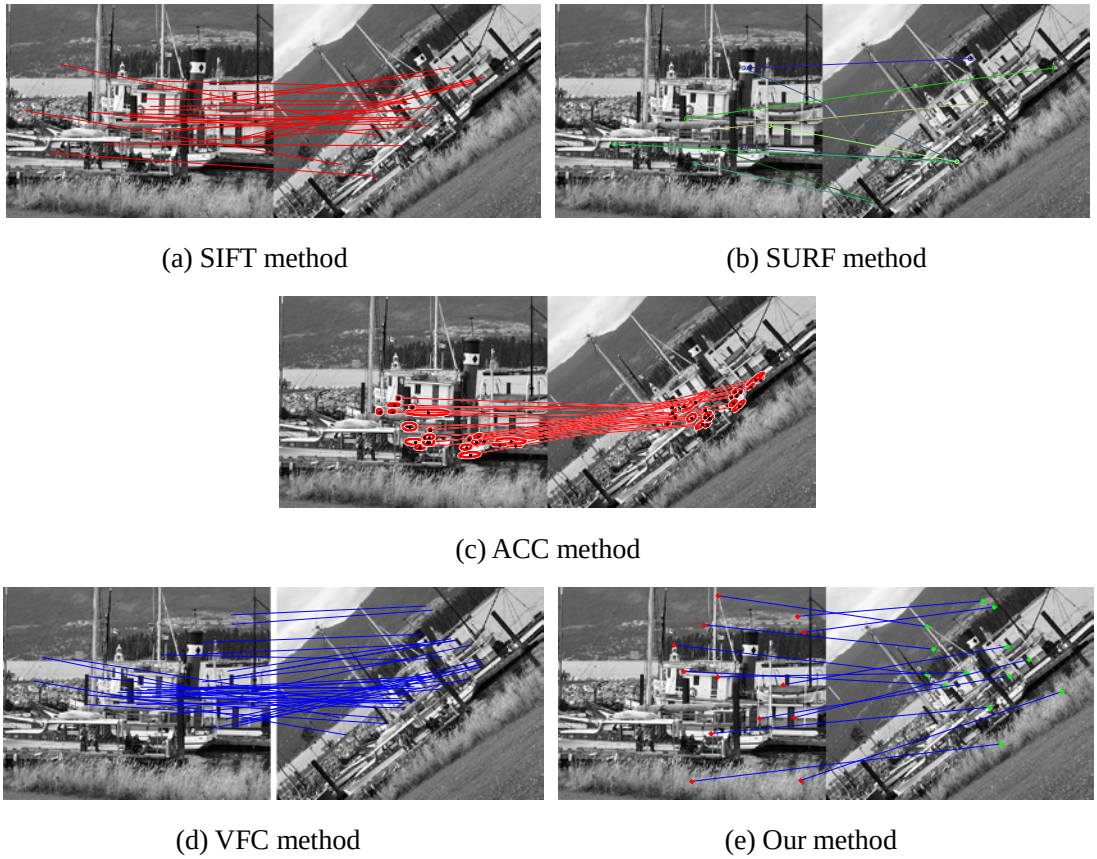

(a) SIFT method (b) SURF method

(c) ACC method

(d) VFC method (e) Our method

Fig. 11: Matching results for the 0^{th} and 2^{nd} frame of the Boat image sequence under zoom and rotation: (a) SIFT method, (b) SURF method, (c) ACC method, (d) VFC method, (e) Our method.

Before verifying the matching performance of the proposed method, we first test the matching performance according to different images of ACC method and VFC method as shown in Fig. 10. Fig. 10 (a) and (c) show the matching results based on ACC method, from which Fig. 10 (a) achieves a one-to-one correspondence. However, there are many mismatches, such as the top left corner and lower right corner, as shown in Fig. 10 (c). On the other hand, Fig. 10 (b) and (d) produce different matching results based on VFC method, which produces some mismatches and achieves a one-to-one correspondence, respectively. From these experimental results,

we know that the ACC and VFC method have their own merits for different types of images.

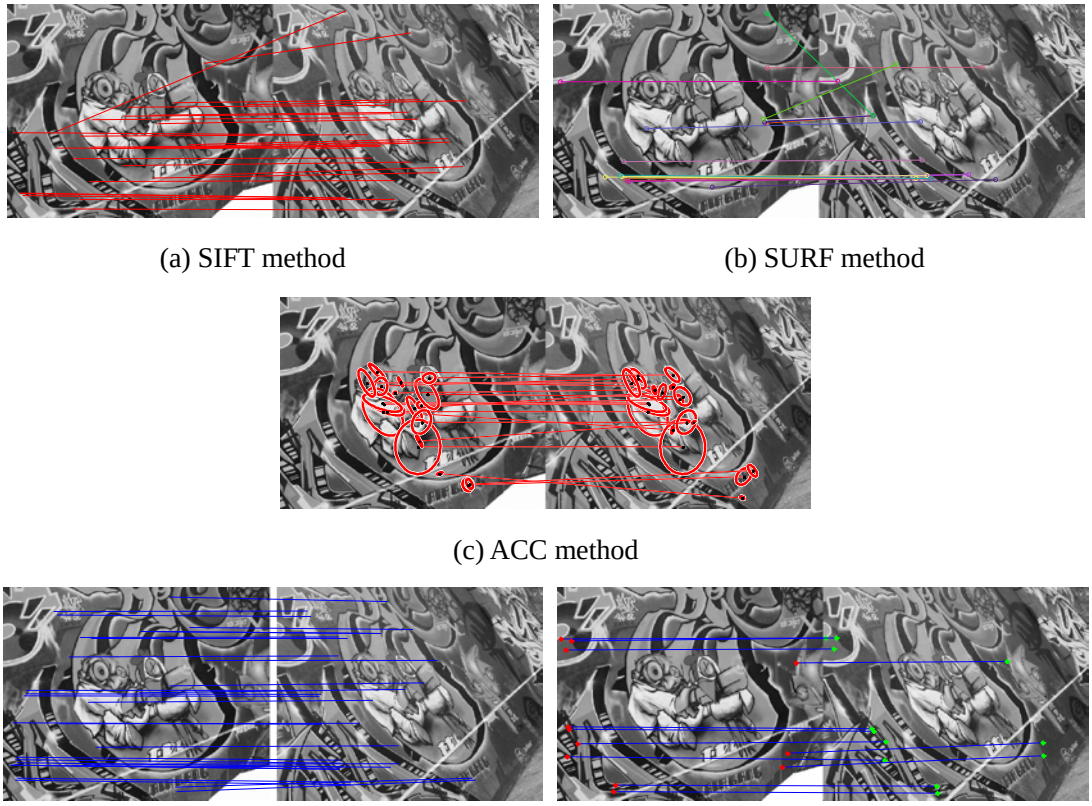

(a) SIFT method (b) SURF method

(c) ACC method

(d) VFC method (e) Our method

Fig. 12: Matching results for 2nd and 4th frame of the Graffiti image sequence under viewpoint: (a) SIFT method, (b) SURF method, (c) ACC method, (d) VFC method, (e) Our method.

To demonstrate the validity of the proposed method, we apply it to public image datasets obtained from [56] which are used to test the robustness to large scale and viewpoint changes by using the Harris-Laplace detector [57]; because, the Harris detector is vulnerable to scale. The experiments are conducted on two image sequences comparing the proposed method with SIFT method, SURF method, ACC method and VFC method to show the proposed method is robust to large scale and viewpoint changes. The comparisons of matching results for two image sequences are shown in Fig. 11 and Fig. 12. It is can be seen that all the methods achieve better correspondence for the Boat image sequence except for the SURF method as shown in Fig. 11, but the computation time is completely different as listed in Table 3. For the Graffiti image sequence, the SIFT method (distRatio=0.52 (default)), SURF method

(Options.tresh=0.0001(default)) and ACC method produce some mismatches as shown in Fig. 12 (a), Fig. 12 (b) and Fig. 12 (c). In contrast, the proposed method and VFC method also produce better matching results. But the proposed method uses the least time for matching compared to the other methods, which further indicates that the proposed method is advantageous considering both accuracy and computation time.

TABLE 3: Comparison of Computation Time and Correct Correspondences Rate for the Different Methods.

Figures, time (seconds) and correct correspondences rate (%)		Methods				
		SIFT	SURF	ACC	VFC	Our method
Fig. 11	seconds	33.5122	8.6635	3.9902	4.7228	3.1185
	%	22(100.0%)	2(22.22%)	22(100.0%)	36(100.0%)	13(100.0%)
Fig. 12	seconds	11.5766	18.1376	4.2221	4.3289	2.6213
	%	25(92.59%)	9(50.00%)	14(73.68%)	30(100.0%)	12(100.0%)

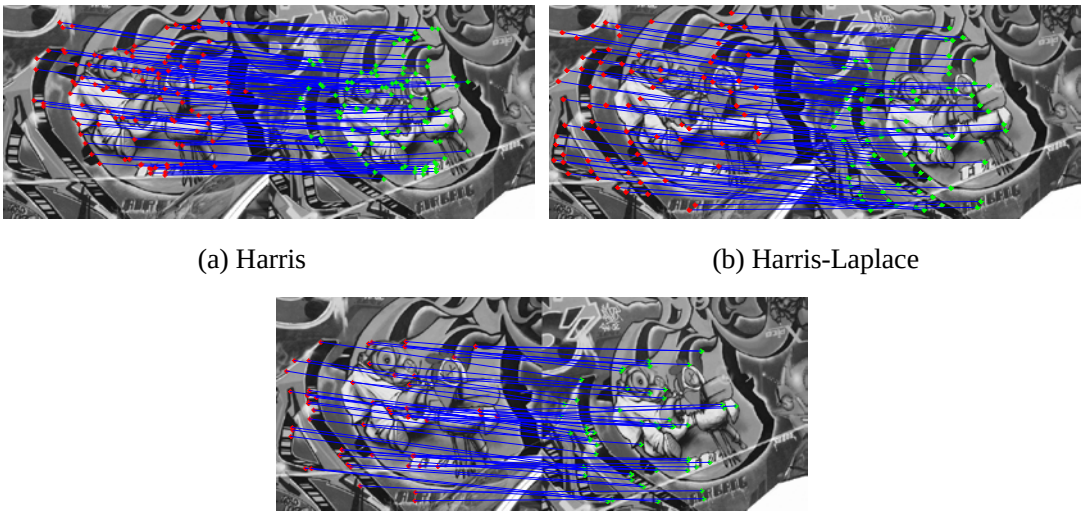

(a) Harris (b) Harris-Laplace

(c) BRISK

Fig. 13: Matching performance for 1st and 2nd frame of the Graffiti image sequence with different feature detector operators: (a) Harris, (b) Harris-Laplace, (c) BRISK.

In order to further test the effectiveness of the proposed method, we combine it with other feature detector operators, such as Harris-Laplace [57] and BRISK [58], to public image datasets to verify that the proposed method can also achieve good correspondence. Fig 13 shows the matching results based on the proposed method

with Harris operator, Harris-Laplace operator and BRISK operator, which indicates that the proposed method can produce better matching results. Some feature points extracted are not very accurate by the Harris detector operator as shown in Fig. 13 (a), but the proposed method can still achieve good matching. In contrast, the Harris-Laplace and BRISK can detect more accurate feature points for much better correspondence, and the performance of Harris-Laplace and BRISK is better than Harris. The BRISK detects some features points which are very close each other, which can produce two-to-one correspondences, but the correspondence is also very accurate. Table 4 gives the accuracy and computation time for the proposed method after combining other feature detector operators, which indicates that the proposed method can achieve better correspondence.

TABLE 4: Comparison of Accuracy and Computation Time for the Different Detector Operators.

Accuracy and Time	The proposed method combining different detector operators		
	Harris	Harris-Laplace	BRISK
Accuracy (%)	95.92(%)	100.00(%)	96.36(%)
Time (s)	2.7028	2.9385	2.6086

5. Conclusion and future work

We presented a novel feature matching method based on principal feature components by stochastic perturbation of a weighted graph, which is computationally efficient. The proposed method obtained the eigenvectors by perturbing the matrix of a sensed weighted graph model. This matrix can be regarded as a modal matrix, with some elements of each row of the modal matrix being feature components of feature points based on eigen-decomposition. Our method can capture accurate correspondences in different types of images and is robust under translation, rotation and scaling, as well as in the presence of outliers and under illumination variations. Experimental results on different types of images are very encouraging and

demonstrate that the proposed method outperforms other algorithms in both accuracy and computational time. In future work we will investigate how to compute the optimal principal feature component values of a weighted graph. Automatically choosing the representative feature points is another challenging problem in image registration that we plan to address.

6. Acknowledgement

This work is supported in part by Alberta Innovates Technologies Futures (AITF), the Natural Sciences and Engineering Research Council (NSERC), the National Natural Science Foundation of China under Grant No. 61363049, the Project funded by China Postdoctoral Science Foundation under Grant Nos. 2014M550881, 2015T80155, the Open Project Program of the State Key Laboratory of Management and Control for Complex Systems under Grant No. 20140101, the Scientific Research Fund of Jiangxi Provincial Education Department under Grant No. GJJ14541, the Open Project Program of the Key Laboratory of Nondestructive Testing, Ministry of Education under Grant No. ZD201429007 and Doctor Scientific Research Starting Foundation under Grant No. EA201307044. The authors would like to thank Dr. L. He, Department of Computing Science, University of Alberta, for providing his RANSAC code.

References

[1] L. J. Grady, and J. R. Polimeni, Discrete Calculus: Applied Analysis on Graphs for Computational Science, Springer, 2010.

[2] S. Umeyama, “An eigendecomposition approach to weighted graph matching problems,” *IEEE Transactions on Pattern Analysis and Machine Intelligence*, vol. 10, no. 5, pp. 695−703, 1988.

[3] G. L. Scott, and H. C. Longuet-Higgins, “An algorithm for associating the features of two images,” *Proceedings of the Royal Society of London*, B-244, pp. 21−26, 1991.

[4] L. S. Shapiro, and J. M. Brady, “Feature-based correspondence: An eigenvector approach,” *Image and Vision Computing*, vol. 10, no. 5, pp. 283−288, 1992.

[5] S. Gold, and A. Rangarajan, “A graduated assignment algorithm for graph matching,” *IEEE Transactions on Pattern Analysis and Machine Intelligence*, vol. 18, no. 4, pp. 377−388, 1996.

[6] J. Shi, and J. Malik, “Normalized cuts and image segmentation,” *IEEE Transactions on Pattern Analysis and Machine Intelligence*, vol. 22, no. 8, pp. 888−905, 2000.

[7] L. Grady, “Random walks for image segmentation,” *IEEE Transactions on Pattern Analysis and Machine Intelligence*, vol. 28, no. 11, pp. 1−17, 2006.

[8] S. Belongie, J. Malik, and J. Puzicha, “Shape matching and object recognition using shape contexts,” *IEEE Transactions on Pattern Analysis and Machine Intelligence*, vol. 24, no. 4, pp. 509−522, 2002.

[9] V. Jain, and H. Zhang, “Robust 3D shape correspondence in the spectral domain,” *IEEE International Conference on Shape Modeling and Applications*, pp. 118−129, 2006.

[10] Z. Tu, S. Zheng, and A. L. Yuille, “Shape matching and registration by data-driven EM,” *Computer Vision and Image Understanding*, vol. 103, no. 3, pp. 290−304, 2007.

[11] D. Mateus, R. Horaud, D. Knossow, F. Cuzzolin, and E. Boyer, “Articulated shape matching using Laplacian eigenfunctions and unsupervised point registration,” *IEEE Conference on Computer Vision and Pattern Recognition*, pp. 1523–1530, 2008.

[12] O. van Kaick, H. Zhang, G. Hamarneh, and D. Cohen-Or, “A survey on shape correspondence,” *Computer Graphics Forum*, vol. 30, no. 6, pp. 1681–1707, 2011.

[13] M. Reuter, “Hierarchical shape segmentation and registration via topological features of Laplace-Beltrami eigenfunctions,” *International Journal of Computer Vision*, vol. 89, no. 2-3, pp. 287–308, 2009.

[14] T. Tlusty, “A relation between the multiplicity of the second eigenvalue of a graph Laplacian, Courant’s nodal line theorem and the substantial dimension of tight polyhedral surfaces,” *Electronic Journal of Linear Algebra*, vol. 16, pp.

315–324, 2010.

[15] A. Ardeshir Goshtasby, Image Registration: Principles, Tools and Methods, Advances in Computer Vision and Pattern Recognition Springer, 2012.

[16] M. Carcassoni, and E. R. Hancock, “Spectral correspondence for point pattern matching,” *Pattern Recognition*, vol. 36, no. 1, pp. 193−204, 2003.

[17] M. Leordeanu, and M. Hebert, “A spectral technique for correspondence problems using pairwise constraints,” *Proc. Int’l Conf. Computer Vision*, 2005.

[18] T. Cour, P. Srinivasan, and J. Shi, “Balanced graph matching,” *Proc. Conf. Neural Information Processing Systems*, 2006.

[19] J. Tang, D. Liang, N. Wang, and Y. Z. Fan, “A Laplacian spectral method for stereo correspondence,” *Pattern Recognition Letters*, vol. 28, no. 12, pp. 1391−1399, 2007.

[20] C. C. Leng, Z. Tian, J. Li, and M. T. Ding, “Image registration based on matrix perturbation analysis using spectral graph,” *Chinese Optics Letters*, vol. 7, no. 11, pp. 996−1000, 2009.

[21] A. Egozi, Y. Keller, and H. Guterman, “Improving shape retrieval by spectral matching and meta similarity,” *IEEE Transactions on Image Processing*, vol. 19, no. 5, pp. 1319–1327, 2010.

[22] H. Zhang, O.Van Kaick, and R. Dyer, “Spectral mesh processing,” *Computer Graphics Forum*, vol. 29, no. 6, pp. 1865–1894, 2010.

[23] H. Lombaert, L. Grady, J. R. Polimeni, and F. Cheriet, “ Fast brain matching with spectral correspondence,” *International Conference on Information Processing in Medical Imaging*, vol. 6801, pp. 660–673, 2011.

[24] R. C. Wilson, and E. R. Hancock, “Structural matching by discrete relaxation,” *IEEE Transactions on Pattern Analysis and Machine Intelligence*, vol. 19, no. 6, pp. 634−648, 1997.

[25] A. D. J. Cross, and E. R. Hancock, “Graph matching with a dual-step EM algorithm,” *IEEE Transactions on Pattern Analysis and Machine Intelligence*, vol. 20, no. 11, pp. 1236−1253, 1998.

[26] B. Luo, and E. R. Hancock, “Structural graph matching using the EM algorithm

and singular value decomposition," *IEEE Transactions on Pattern Analysis and Machine Intelligence*, vol. 23, no. 10, pp. 1120−1136, 2001.

[27] R. Zass, and A. Shashua, "Probabilistic graph and hypergraph matching," *Proc. IEEE Int'l Conf. Computer Vision and Pattern Recognition*, pp.1221−1228, 2008.

[28] Y. Suh, M. Cho, and K. M. Lee, "Graph matching via sequential monte carlo," *In: Fitzgibbon A., et al. (Eds.): ECCV 2012, Part III. LNCS*, vol. 7574, pp. 624–637, 2012.

[29] M. Cho, and K. M. Lee, "Progressive graph matching: Making a move of graphs via probabilistic voting," *IEEE Conference on Computer Vision and Pattern Recognition*, pp. 398–405, 2012.

[30] L. Xu, and I. King, "A PCA approach for fast retrieval of structural patterns in attributed graphs," *IEEE Transactions on Systems, Man, and Cybernetics*, vol. B31, no. 5, pp. 812−817, 2001.

[31] T. Caelli, and S. Kosinov, "An eigenspace projection clustering method for inexact graph matching," *IEEE Transactions on Pattern Analysis and Machine Intelligence*, vol. 26, no. 4, pp. 515−519, 2004.

[32] M. Cho, J. Lee, and K. M. Lee, "Feature correspondence and deformable object matching via agglomerative correspondence clustering," *IEEE 12th International Conference on Computer Vision*, pp. 1280−1287, 2009.

[33] M. A. Fischler, and R. C. Bolles, "Random Sample Consensus: A paradigm for model fitting with applications to image analysis and automated cartography," *Comm. ACM*, vol. 24, no. 6, pp. 381−395, 1981.

[34] P. H. S. Torr, and C. Davidson, "IMPSAC: synthesis of importance sampling and random sample consensus," *IEEE Transactions on Pattern Analysis and Machine Intelligence*, vol. 25, no. 3, pp. 354−364, 2003.

[35] T. Vercauteren, X. Pennec, A. Perchant, and N. Ayache, "Non-parametric diffeomorphic image registration with the demons algorithm," *In: Ayache, N., Ourselin, S., Maeder, A. J. (Eds.) Proc. MICCAI 2007, Part II. LNCS*, vol. 4792, pp. 319–326, 2007.

[36] T. Vercauteren, X. Pennec, A. Perchant, and N. Ayache, "Symmetric log-domain

diffeomorphic registration: A demons-based approach," *In: Proc. MICCAI 2008, Part I. LNCS*, vol. 5241, pp. 754–761, 2008.

[37] M. Cho, J. Lee, and K. M. Lee, "Reweighted random walks for graph matching," *In: Daniilidis, K., Maragos, P., Paragios, N. (Eds.): ECCV 2010, Part V. LNCS*, vol. 6315, pp. 492–505, 2010.

[38] J. Chen, J. Y. Ma, C. C. Yang, L. Ma, and S. Zheng, "Non-rigid point set registration via coherent spatial mapping," *Signal Processing*, vol. 106, pp. 62–72, 2015.

[39] Fan R. K. Chung, Spectral Graph Theory, Providence, RI: American Mathematical Society, 1997.

[40] U. von Luxburg, "A tutorial on spectral clustering," *Statistics and Computing*, vol. 17, no. 4, pp. 395–416, 2007.

[41] X. Bai, and L. J. Latecki, "Path similarity skeleton graph matching," *IEEE Transactions on Pattern Analysis and Machine Intelligence*, vol. 30, no. 7, pp. 1282–1292, 2008.

[42] C. Wang, L. Wang, and L. Q. Liu, "Improving graph matching via density maximization," *IEEE International Conference on Computer Vision*, pp. 3424–3431, 2013.

[43] T. S. Caetano, J. J. McAuley, L. Cheng, Q. V. Le, and A. J. Smola, "Learning graph matching," *IEEE Transactions on Pattern Analysis and Machine Intelligence*, vol. 31, no. 6, pp. 1048–1058, 2009.

[44] J. Y. Ma, J. Zhao, J. W. Tian, X. Bai, Z. W. Tu, "Regularized vector field learning with sparse approximation for mismatch removal," *Pattern Recognition*, vol. 46, no.12, 3519–3532, 2013.

[45] J. Y. Ma, J. Zhao, J. W. Tian, A. L. Yuille, and Z. W. Tu, "Robust point matching via vector field consensus," *IEEE Transactions on Image processing*, vol. 23, no. 4, pp. 1706–1721, 2014.

[46] J. Y. Ma, J. Zhao, J. W. Tian, Z. W. Tu, and A. L. Yuille, "Robust estimation of nonrigid transformation for point set registration," *Proceedings of the IEEE Conference on Computer Vision and Pattern Recognition*, pp. 2147–2154, 2013.

[47] J. Y. Ma, W. C. Qiu, J. Zhao, Y. Ma, A. L. Yuille, and Z. W. Tu, “Robust L_2E estimation of transformation for non-rigid registration,” *IEEE Transactions on Signal Processing*, vol. 63, no. 5, pp.1115–1129, 2015.

[48] J. Y. Ma, J. Zhao, Y. Ma, and J. W. Tian, “Non-rigid visible and infrared face registration via regularized Gaussian fields criterion,” *Pattern Recognition*, vol. 48, no. 3, pp. 772–784, 2015.

[49] Y. H. Liu, L. D. Dominicis, B. G. Wei, L. Chen, and R. R. Martin, “Regularization based iterative point match weighting for accurate rigid transformation estimation,” *IEEE Transactions on Visualization and Computer Graphics*, vol. 21, no. 9, pp. 1058–1071, 2015.

[50] J. G. Sun, Matrix Perturbation Analysis, Beijing: Science Press, 2001.

[51] D. Conte, P. Foggia, C. Sansone, and M. Vento, “Thirty years of graph matching in pattern recognition,” *Graph Matching in Pattern Recognition and Machine Vision*, vol. 18, no. 3, pp. 265−298, 2004.

[52] C. Harris, and M. Stephens, “A combined corner and edge detector,” *Proc. Alvey Vision Conf.*, pp. 147−151, 1988.

[53] http://www.robots.ox.ac.uk/~vgg/data1.html.

[54] D. G. Lowe, “Distinctive image features from scale-invariant keypoints,” *International Journal of Computer Vision*, vol. 60, no. 2, pp. 91–110, 2004.

[55] H. Bay, A. Ess, T. Tuytelaars, and L. V Gool, “Speeded-up robust features (SURF),” *Computer Vision and Image Understanding*, vol. 110, no. 3, pp. 346–359, 2008.

[56] http://lear.inrialpes.fr/people/mikolajczyk/Database/index.html.

[57] K. Mikolajczyk, and C. Schmid, “Scale & affine invariant interest point detectors,” *International Journal of Computer Vision*, vol. 60, no. 1, pp. 63–86, 2004.

[58] S. Leutenegger, M. Chli, and R. Y. Siegwart, “BRISK: binary robust invariant scalable keypoints,” *Proceedings of the IEEE International Conference on Computer Vision*, pp. 2548–2555, 2011.

Chengcai Leng received the Ph.D. degree in Applied Mathematics from Northwestern Polytechnical University, Xi'an, China, in 2012. From September 2010 to September 2011, he was a visiting student at the Department of Computing Science, University of Alberta, Edmonton, Canada. He is a Lecturer in School of Mathematics and Information Science, Nanchang Hangkong University, China. His current research interests include image processing, computer vision and optical molecular imaging.

We Xu received the Ph.D. degree from Northwestern Polytechnical University, Xi'an, China. He is a Professor in the Department of Applied Mathematics, Northwestern Polytechnical University, China. His current research interests include system simulation model and nonlinear stochastic dynamics.

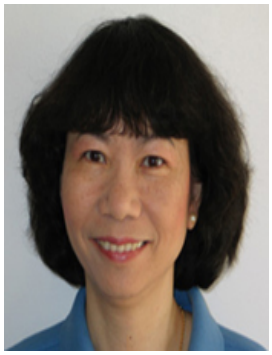

Irene Cheng is the Scientific Director of the Multimedia Research Group, the Director of the Master with Specialization in Multimedia Program and an Adjunct Professor at the University of Alberta, Canada. She received the University of Alberta Alumni Horizon Award in 2008. She was a Co-Founder of the IEEE SMC Society, Human Perception in Multimedia Computing Technical Committee; the Chair of the IEEE Northern Canada Section, Engineering in Medicine and Biological Science Chapter, and the Chair of the IEEE Communication Society, Multimedia Technical Committee 3D Processing, Render and Communication (MMTC) Interest Group, the Director of the Review-Letter Editorial Board of MMTC. She received the TCL Research America Researcher's Award and the Outstanding Leadership Award from MMTC 2014. She is an Associate Editor of the IEEE Transactions on Human-Machine Systems. Her research interests include multimedia computing and transmission, levels-of-detail, 3-D TV, visualization and perceptual quality assessment. In particular, she introduced applying human perception- Just-Noticeable-Difference (JND) and Relative Change-following psychophysical methodology for multi-scale analytic.

Anup Basu (M'90－SM'02) received the Ph.D. degree in computer science from the University of Maryland, College Park. He was a Visiting Professor at the University of California, Riverside, a Guest Professor at the Technical University of Austria, Graz, and the Director at the Hewlett-Packard Imaging Systems Instructional Laboratory, University of Alberta, Edmonton, Canada, where, since 1999, he has been a Professor at the Department of Computing Science, and is currently an iCORE-NSERC Industry Research Chair. He originated the use of foveation for image, video, stereo, and graphics communication in the early 1990s, an approach that

is now widely used in industrial standards. He also developed the first robust (correspondence free) 3-D motion estimation algorithm, using multiple cameras, a robust (and the first correspondence free) active camera calibration method, a single camera panoramic stereo, and several new approaches merging foveation and stereo with application to 3-D TV visualization and better depth estimation. His current research interests include 3-D/4-D image processing and visualization especially for medical applications, multimedia in education and games, and wireless 3-D multimedia transmission.